

PCCP

Accepted Manuscript



This is an *Accepted Manuscript*, which has been through the Royal Society of Chemistry peer review process and has been accepted for publication.

Accepted Manuscripts are published online shortly after acceptance, before technical editing, formatting and proof reading. Using this free service, authors can make their results available to the community, in citable form, before we publish the edited article. We will replace this *Accepted Manuscript* with the edited and formatted *Advance Article* as soon as it is available.

You can find more information about *Accepted Manuscripts* in the [Information for Authors](#).

Please note that technical editing may introduce minor changes to the text and/or graphics, which may alter content. The journal's standard [Terms & Conditions](#) and the [Ethical guidelines](#) still apply. In no event shall the Royal Society of Chemistry be held responsible for any errors or omissions in this *Accepted Manuscript* or any consequences arising from the use of any information it contains.

Quasi-particle energies and optical excitations of hydrogenated and fluorinated germanene

Huabing Shu, Yunhai Li, Shudong Wang, Jinlan Wang*

Using density functional theory, G_0W_0 method and Bethe-Salpeter equation calculations, we systematically explore the structural, electronic and optical properties of hydrogenated and fluorinated germanene. The hydrogenated/fluorinated germanene tend to form chair and zigzag-line configurations and their electronic and optical properties show close geometry dependence. The chair hydrogenated/fluorinated and zigzag-line fluorinated germanene are direct band-gap semiconductors, while the zigzag-line hydrogenated germanene owns an indirect band-gap. Moreover, the quasi-particle corrections are significant and strong excitonic effects with large exciton binding energies are observed. Moreover, the zigzag-line hydrogenated/fluorinated germanene show highly anisotropic optical responses, which may be used as good optical linear polarizers.

Department of Physics, Southeast University, Nanjing, 211189, China

* *Electronic mail:* jlwang@seu.edu.cn.

1 Introduction

Graphene, atomically thin two-dimensional materials, has exhibited unique electronic and optical properties¹⁻⁴ and holds great potential applications in future electronics⁵ and optoelectronics⁶. Nevertheless, due to its semi-metallic nature, the introduction of finite band-gap into graphene is essential.⁷ Several approaches have been used to open the band-gap of graphene.⁸ One of efficient ways is chemical functionalization of graphene. Available theoretical and experimental studies⁹⁻¹³ have both demonstrated that fully hydrogenation and fluorination of graphene can successfully introduce a significant band-gap of 3.5 eV and 3.07 eV, respectively. Other functional groups such as benzoyl¹⁴, nitrobenzene¹⁵ can also form covalent bonds with carbon atoms of graphene and induce sp^2 - sp^3 hybridization transformation, leading to the opening of band-gap through the Fermi level shift in the graphene.¹⁶⁻¹⁷

Silicon (Si) and germanium (Ge), belonging to the same group as carbon in the periodic table, have been predicted to form nanosheet analogous to graphene, namely silicene and germanene¹⁸⁻²¹. Theoretical investigations²²⁻²⁵ have indicated that they have similar band structure with graphene, in which the zero-gap semi-metallic behavior appears with Dirac-like electronic excitation. Most recently, monolayer silicene²⁶ and germanene²⁷ have been synthesized on silver and gold substrates via epitaxial grown method, respectively. Theoretical studies have further revealed that fully hydrogenated silicene forms chair-like structure with an indirect band-gap of about 2.1 eV²⁸⁻³⁰, while fully fluorinated silicene prefers a zigzag-line buckling configuration with a direct band-gap of 0.7 eV²⁹. These silicene derivatives also

exhibit intriguing optical absorption properties such as strong excitonic effects with large exciton binding energies 1.07 eV and 1.48 eV for fully hydrogenated/fluorinated silicene³⁰, respectively. Fully hydrogenated germanene also shows strong excitonic effects and the exciton binding energy is about 0.6 eV³¹.

In this paper, we employ density functional theory (DFT), G_0W_0 method and Bethe-Salpeter equation (BSE) to investigate the quasi-particle (QP) band structure and optical absorption spectrum of fully hydrogenated and fluorinated germanene. The stability of different structures and their influence to the QP band structure and excitonic effects are also addressed. Our calculations show that the chair hydrogenated/fluorinated and zigzag-line fluorinated germanene are direct band-gap semiconductors, while the zigzag-line hydrogenated germanene possesses an indirect band-gap. More interestingly, binding energies of the first bound excitation are as large as 0.75 eV and 0.73 eV in chair hydrogenated/fluorinated germanene and the high buckling zigzag-line hydrogenated/fluorinated germanene exhibit highly anisotropic optical responses.

2 Computational methods

We first performed local density approximation (LDA) calculations using the Perdew and Wang functional,³² implemented in Quantum Espresso code,³³ to optimize hydrogenated and fluorinated germanene with different configurations and obtain their ground-state electronic structures. Plane-wave basis set with an energy cutoff of 60 Ry, $18 \times 18 \times 1$ k -point sampling and norm-conserving pseudopotentials³⁴ for

ion-electron interactions were employed. A vacuum region of 20 Å along the direction perpendicular to the sheet was used to avoid interaction between adjacent cells. The atomic structures were fully relaxed with the total energy converged to less than 10^{-4} eV and the forces acting on each atom less than 0.01 eV/Å.

Based on the electronic ground-state wave function and eigenvalues obtained from LDA, the quasi-particle energies were then calculated to obtain the accuracy electronic band structure within the *GW* approximation³⁵⁻³⁸ by the following equation:

$$E_{nk}^{QP} = \varepsilon_{nk}^{KS} + Z_{nk}(\varepsilon_{nk}^{KS}) \langle \psi_{nk} | \Sigma(\varepsilon_{nk}^{KS}) - V_{XC}^{LDA} | \psi_{nk} \rangle, \quad (1)$$

where $Z_{nk}(\varepsilon_{nk}^{KS}) = (1 - \frac{\partial \Sigma}{\partial E} |_{\varepsilon_{nk}^{KS}})^{-1}$, Z_{nk} is the renormalization factor. V_{XC}^{LDA} is the exchange-correlation potential. Self-energy Σ is the product of the non-interacting one-electron Green's function G_0 and the screened Coulomb potential W_0 constructed by the Godby-Needs plasmon-pole approximation (PPA)³⁹⁻⁴⁰ in this study, *i.e.*, $\Sigma = iG_0W_0$.

Finally, the optical absorption spectra including electron-hole interaction were calculated via the Bethe-Salpeter equation,⁴¹⁻⁴³

$$(E_{ck}^{qp} - E_{vk}^{qp})A_{vck}^S + \sum_{k'v'c'} \langle vck | K^d + 2K^x | v'c'k' \rangle A_{v'c'k'}^S = \Omega_s A_{vck}^S, \quad (2)$$

where v , c , and \mathbf{k} indicate the valence band, conduction band and \mathbf{k} vector respectively; E_{ck}^{qp} and E_{vk}^{qp} are the quasi-particle energies for the electron and hole states; $\langle vck |$ and $| v'c'k' \rangle$ refer to the quasi-electron and quasi-hole states, respectively. A_{vck}^S and Ω_s are the electron-hole amplitudes and the excitation energy, respectively. K^d , related to the screened Coulomb interaction W_0 , is the direct interaction term which is responsible for the attractive nature of electron-hole

interaction. K^x is the repulsive exchange term of the electron-hole interaction which includes the bare Coulomb interaction V .

In G_0W_0 and BSE calculations, the Coulomb interaction along the direction perpendicular to the sheet was truncated at 25 a.u. in order to avoid spurious interaction between periodic images. 360 and 384 conduction bands were used to construct the dielectric matrices and self-energy operator. The energy cutoffs for the exchange and correlation of the self-energy operator were 8 Ry and 50 Ry respectively. Five valence bands and ten conduction bands were taken into account to construct the electron-hole interaction kernel. A k -point grid of $24 \times 24 \times 1$ was used for the G_0W_0 calculation and a denser $48 \times 48 \times 1$ k -point grid for BSE calculation. These parameters ensure the convergence of G_0W_0 gap and absorption spectra within 0.08 eV. The G_0W_0 and BSE calculations were performed using the YAMBO³⁸ program package.

3 Results and discussions

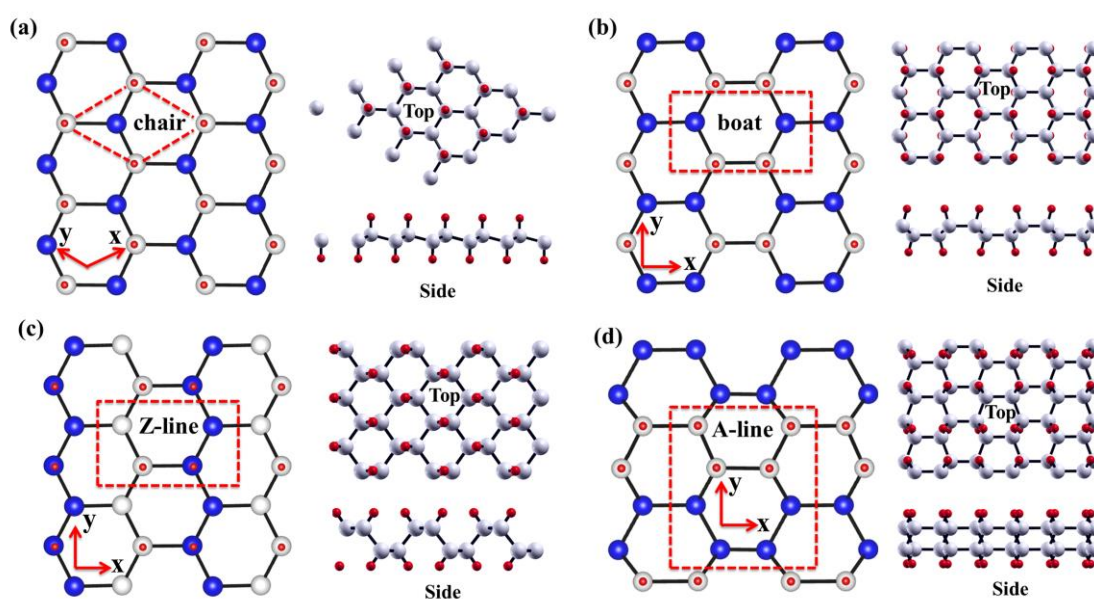


Figure 1. Structures of germanane and fluorogermanene in (a) chair, (b) boat, (c)

zigzag-line, (d) armchair-line configurations. The blue and white spheres indicate germanium atoms at different altitudes, while the red ones refer to hydrogen or fluorine atoms, respectively. Red diamond and rectangle represent the primitive cell. (a)-(d) Right: Top (upper panel) and side views (lower panel) of the optimized structures for fluorogermanene.

3.1 Structure and stability of hydrogenated and fluorinated germanene

Following the naming convention for graphene and graphane¹¹, we refer to the hydrogenated and fluorinated germanene sheets as germanane and fluorogermanene, respectively. As shown in the left panels of Figure 1(a)-1(d), four possible buckled configurations analogous to graphane⁴⁴ are considered for germanane and fluorogermanene, respectively. The chair configuration has a buckling alternated by the single Ge atom. The boat configuration has a buckling alternated with the pair Ge atoms. Carefully examination shows that the chair/boat germanane and chair fluorogermanene are all biaxially strained; while the boat fluorogermanene is uniaxially strained. The zigzag-line (Z-line) and the armchair-line (A-line) configurations have the buckling alternated by the zigzag and armchair lines of Ge atoms, respectively. The optimized structures of fluorogermanene are displayed in right panels of Figure 1(a)-(d), which the germanane ones are very similar. Their structural and energetic information together those of germanene are summarized in Table 1. Our results of the chair germanene and germanane are in good agreement with other DFT calculations^{18, 22, 31, 45}, and the equilibrium lattice constant (b_{zig}) 3.95 Å for germanane, is also in good accordance with the available experimental result of

3.98 Å⁴⁶⁻⁴⁷. Compared with pristine germanene, the Ge-Ge bond lengths (d_{Ge-Ge}) in germanane and fluorogermanene are lengthened slightly by about 1.68% ~ 3.07% and 2.36% ~ 4.06% due to the formation of Ge-H and Ge-F bonds, respectively. The chair germanane and fluorogermanene both have relatively low buckling height (Δ_z) of 0.72 Å and 0.61 Å, while its Z-line configurations possess quite high buckling height of 1.971 Å and 1.957 Å (see Table 1), respectively. The large buckling heights decrease the cell parameter a_{arm} significantly, which it can be even shrank by about 16.6% with respect to ($3.92 \times \sqrt{3} \approx 6.79$ Å) germanene. The binding energies and formation energies were calculated to evaluate the stability of the germanane and fluorogermanene. The binding energy (E_B) is defined as $E_B = (N_{Ge} \times E_{Ge-atom} + N_X \times E_{X-atom} - E_{total}) / N$, where N_{Ge} , N_X , N are the number of atoms of Ge, X (hydrogen or fluorine), and the total number of atoms in unit cell, $E_{Ge-atom}$ or E_{X-atom} is the energy of Ge, H or F atom, E_{total} is the total energy of germanane or fluorogermanene. For germanane, the binding energies of four different configurations are 2.575 (Chair), 2.560 (Boat), 2.566 (Z-line), and 2.563 (A-line) eV per atom, while they are 5.205 (Chair), 5.190 (Boat), 5.197 (Z-line), and 5.194 (A-line) eV per atom for fluorogermanene, respectively. The large E_B indicates that fluorogermanene is very stable. The formation energy (E_F) is calculated as well, defined as $E_F = (E_{total} - E_l - \frac{N_X}{2} E_{X_2}) / N$, where E_l is the total energy of germanene, and E_{X_2} is the energy of a H₂ or F₂ molecule. The energies both follow the order of $E_F(\text{chair}) < E_F(\text{Z-line}) < E_F(\text{A-line}) < E_F(\text{Boat})$ for germanane and fluorogermanene. Moreover, the formation energies of germanane and fluorogermanene are more negative, especially for

fluorogermanene, than those of hydrogenated or fluorinated graphene⁴⁷, suggesting that they could be feasible experimentally.

Table 1. Structural and energetic parameters for the germanene/ fluorogermanene of four configurations and germanene: cell parameters a_{arm} (Å), b_{zig} (Å), bond length d_{Ge-Ge} (Å), d_{Ge-X} ($X = H$ or F) (Å), buckling height Δ_z (Å), binding energy E_B (eV/atom) and formation energy E_F (eV/atom).

	Germanene		Germanane			Fluorogermanene			
	Chair	Chair	Boat	Z-line	A-line	Chair	Boat	Z-line	A-line
a_{arm}	——	——	6.670	5.700	6.400	——	6.910	5.660	6.560
b_{zig}	3.920	3.950	3.850	3.890	6.720	4.100	4.090	3.900	6.700
d_{Ge-Ge}	2.340	2.390	2.414	2.382	2.380	2.400	2.439	2.430	2.394
d_{Ge-X}	——	1.529	1.530	1.530	1.530	1.700	1.698	1.693	1.693
Δ_z	0.616	0.720	1.032	1.971	1.940	0.610	0.876	1.957	1.956
E_B	4.675	2.575	2.560	2.566	2.563	5.205	5.190	5.197	5.194
E_F	——	-0.270	-0.254	-0.262	-0.260	-1.849	-1.821	-1.842	-1.834

3.2 Electronic structure and optical properties of chair germanene and fluorogermanene

We first investigate the electronic structure of the chair germanene, germanane and fluorogermanene at LDA level and display their band structure, projected density of states and charge density in Figure 2. As shown from the figure, germanene owns a zero band-gap, corresponding to the semi-metallic property. Its valence band

maximum (VBM) and conduction band minimum (CBM) coincide at K point, which are mainly contributed by the $4p_z$ orbitals of Ge atoms, and the corresponding charge densities center around one of two nonequivalent Ge atoms. The chair germanane is a semiconductor with a direct band-gap of 1.38 eV at Γ point, which stems from the hydrogenation induced sp^2 - sp^3 hybridization of Ge atoms. Further, the charge density distribution indicates both the VBM and CBM states originate from the contribution of Ge- $4p$ states, as shown in Figure 2(d). Similarly, the chair fluorogermanene owns a direct band-gap of 0.19 eV at Γ point. The CBM in germanane and fluorogermanene both consists of sp^3 -like hybridization orbitals of Ge atoms (Figure 2(c) & (e) right). The VBM mostly originates from the combination of Ge- $(4p_x+4p_y)$ and F- $(2p_x+2p_y)$ orbitals for fluorogermanene, while that of germanane is mainly from Ge- $(4p_x+4p_y)$. Moreover, all valence bands in fluorogermanene include F- $(2p_x+2p_y)$ orbitals (see Figure 2(e) right), which may induce the significant shift of VBM relative to the CBM in comparison with that of germanane and eventually lead to the small band-gap of fluorogermanene.

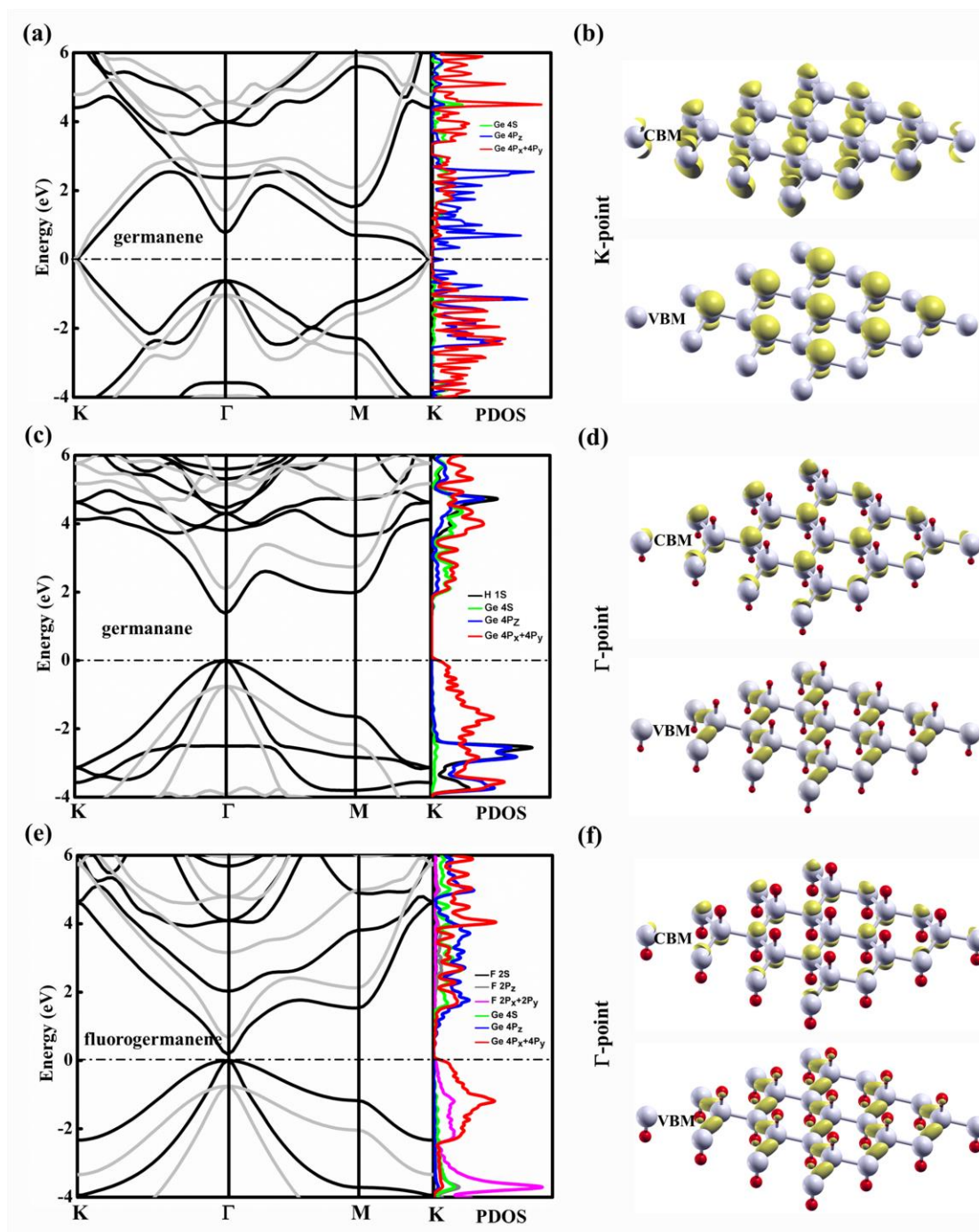


Figure 2. (a), (c), (e): Band structure and projected density of states of germanene, germanane and fluorogermanene with chair configuration; (b), (d), (f): Charge density of VBM and CBM; an isovalue of $0.0025 \text{ e}/\text{\AA}^3$ is used. The black and grey solid lines represent the results from the LDA and G_0W_0 calculations, respectively. The energy of VBM is shifted to 0 eV.

The quasi-particle corrections at GW level for germanane and fluorogermanene are presented in Figure 2(c) & (e). Compared with LDA results, the corrected conduction band is shifted up, while the valence band is shifted down. The opening of the band-gaps is sizeable (more than 100% compared to the LDA gaps) and the QP band-gaps of germanane and fluorogermanene increase to 2.81 eV and 1.43 eV (see Table 2), respectively. Such significant QP corrections are the consequence of reduced electronic screening which can significantly enhance the Coulomb interaction in germanane and fluorogermanene. Similar significant QP corrections in the atomically thin materials, have been observed in hydrogenated and fluorinated graphene as well.^{30-31, 49}

Table 2. Band-gap E_{g-LDA} (eV) at DFT-LDA level, E_{g-GW} (eV) at GW level, excitation energy E_{e-A}^1 and binding energy E_{b-A}^1 (eV) of the first resonant or bound exciton of germanane or fluorogermanene, which is defined as the difference between the excitation energy and the QP energy difference. The x and y indicate the direction of incident light polarized.

	Configuration	E_{g-LDA}	E_{g-GW}	E_{e-A}^1	E_{b-A}^1
germanane	Chair	1.38	2.81	2.06	0.75
	Zigzag-line	1.91 ^(indirect)	3.65 ^(indirect)	4.33 (x)	0.42
		2.19 ^(direct)	3.83 ^(direct)	3.15 (y)	0.95
fluorogermanene	Chair	0.19	1.43	0.70	0.73
	Zigzag-line	0.71	2.45	1.94 (x)	2.37
				0.72 (y)	2.80

The optical absorption spectra without the electron-hole interaction ($GW+RPA$) and with the electron-hole interaction ($GW+BSE$) from the solution of the Bethe-Salpeter

equation³⁸, are displayed in Figure 3. Considering the depolarization effects perpendicular to the plane, we only focus on the optical absorption for light polarization parallel to the germanane (fluorogermanene) surface. Our calculations show that the optical absorption spectra are very similar for the incident light polarized along x and y directions at *GW*+RPA or *GW*+BSE level. So, we only present the absorption spectra for the incident light polarized along x direction shown in Figure 1(a). As clearly shown in Figure 3(a) & (b), the excitonic effects dramatically reshape the spectral profile comparing with the single-particle optical spectra. When the self-energy corrections are included, the entire spectrum shifts to the high energy scope (blue-shift); while it is pushed back as the electron-hole (*e-h*) interactions are included. For germanane, the first bound exciton A^1 , corresponding to the first absorption peak, is observed at 2.06 eV (see Figure 3(a)), which is originated from two energetically degenerate excitons with an *e-h* binding energy of 0.75 eV (see Table 2). This indicates that the germanane is very promising for the observation of excitonic effects in the visible light range. In the case of fluorogermanene, one strong absorption peaks is observed at 0.70 eV (see Figure 3(b)), which is also from two energetically degenerate excitons with a large *e-h* binding energy of 0.73 eV (see Table 2). The binding energies of these excitons in germanane and fluorogermanene are comparable to those found in other monolayer semiconductors and 1D nanostructures.⁵⁰⁻⁵³ The reduced dimensionality and weakened electronic screening are primary factors for fostering such enhanced excitonic effects. In addition, in comparison with resonant excitons in germanene,⁵⁴ the first bound exciton with the

almost same binding energy in germanane and fluorogermanene is of particular interest due to the large binding energy, large oscillator strength, as well as their two-dimensional character, which make germanane and fluorogermanene hold the promise for possible important applications in optoelectronics.

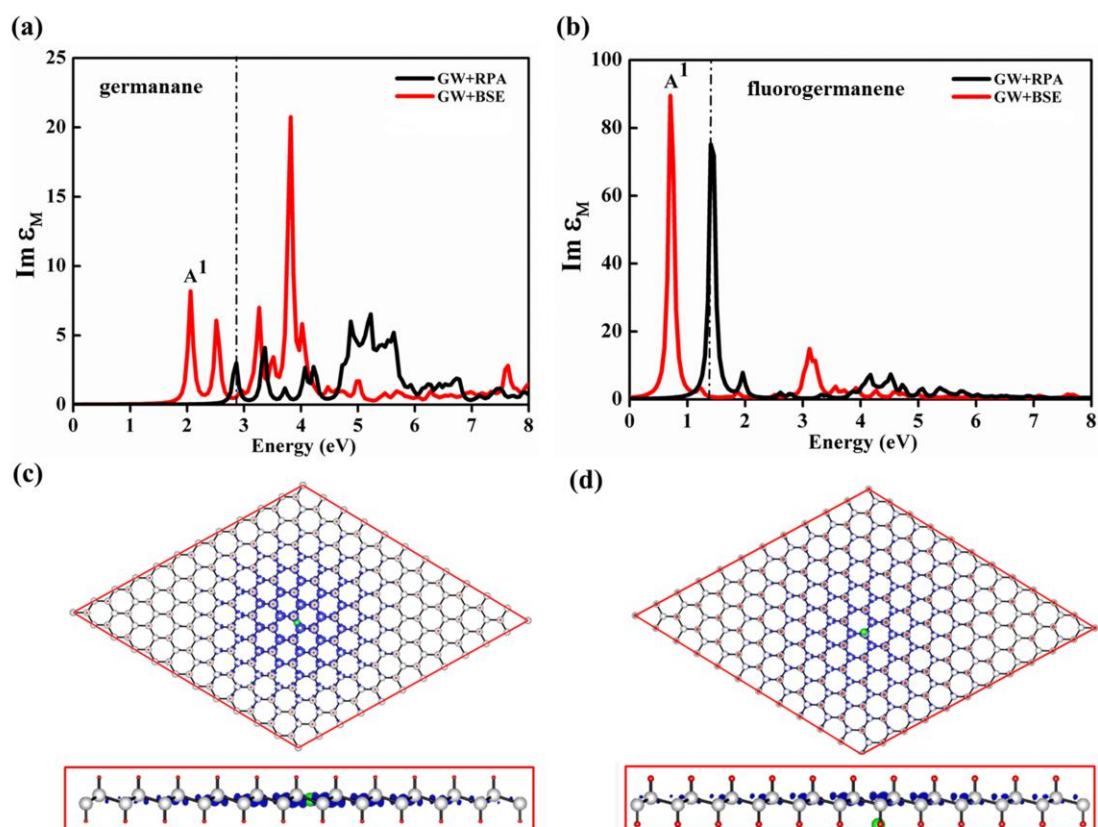


Figure 3. (a), (b): Optical absorption spectra for light polarization parallel to the chair germanane (fluorogermanene) sheet without (black line) and with (red line) the e-h interaction, *i.e.* $GW+RPA$ and $GW+BSE$. A Lorentzian broadening of 0.05 eV was adopted. A^1 denotes the first bound exciton. The vertical black dash dot lines indicate the positions of the lowest direct QP gap. Top and side views of the first bound exciton wave functions for germanane (c) and for fluorogermanene (d), where the hole position (green dot) is fixed on Ge-Ge bond for germanane and fluorine atom for fluorogermanene.

To gain further insight of the optical spectra, we explore the excitonic wave function related to the main peaks of absorption spectra. The excitonic wave function can be written as

$$|\Psi^S(r_e, r_h)\rangle = \sum_{c, v, k} A_{cvk}^S \Psi_{cvk}^S(r_e, r_h), \quad (3)$$

where r_e and r_h are the real space electron and hole coordinate, respectively. The Ψ is the quasi-particle wave function. The coefficients A_{cvk}^S are obtained by diagonalizing the Hamiltonian of Bethe-Salpter equation. To represent the six coordinate function, we fixed the hole position on the Ge-Ge bond for germanane (fluorine atom for fluorogermanene), and projected the modulus squared of the real-space quasi-particle wave function ($|\Psi^S[r_e, r_h = (0,0,0)]|^2$) onto the x-y plane. For germanane and fluorogermanene, electron probability distribution $|\Psi^S(r_e, r_h)|^2$ of the first bound exciton is shown in Figure 3(c) & (d), respectively. The wave function pictures of these bound excitons show an obvious damping nature, which is an indication of the bound between quasi-electron and quasi-hole governed by the excitonic effects. Moreover, the exciton spreads in a relatively localized space with an exciton radius of $\sim 17 \text{ \AA}$ and $\sim 24 \text{ \AA}$ for germanane and fluorogermanene, respectively. Actually, the exciton radius is closely related to the exciton binding energy. According to hydrogen atom model, $E = E_g - C e^2/2r$, where E is excitonic energy, E_g is the band-gap, $-e^2/2r$ is the energy eigenvalues of the hydrogen atom ground state, C is a constant and r is Bohr radius, one can conclude that the larger the Bohr radius, the smaller the $(E_g - E)$. As the exciton radius and binding energy can be analogous to the Bohr radius r and $(E_g - E)$ of hydrogen atom model, we can easily draw a conclusion that for a smaller

radius, the electron and the hole will be confined within a narrower area, thus the interaction between them is enhanced, and eventually results in larger binding energy.

3.3 Electronic structure and optical properties of Z-line germanane and fluorogermanene

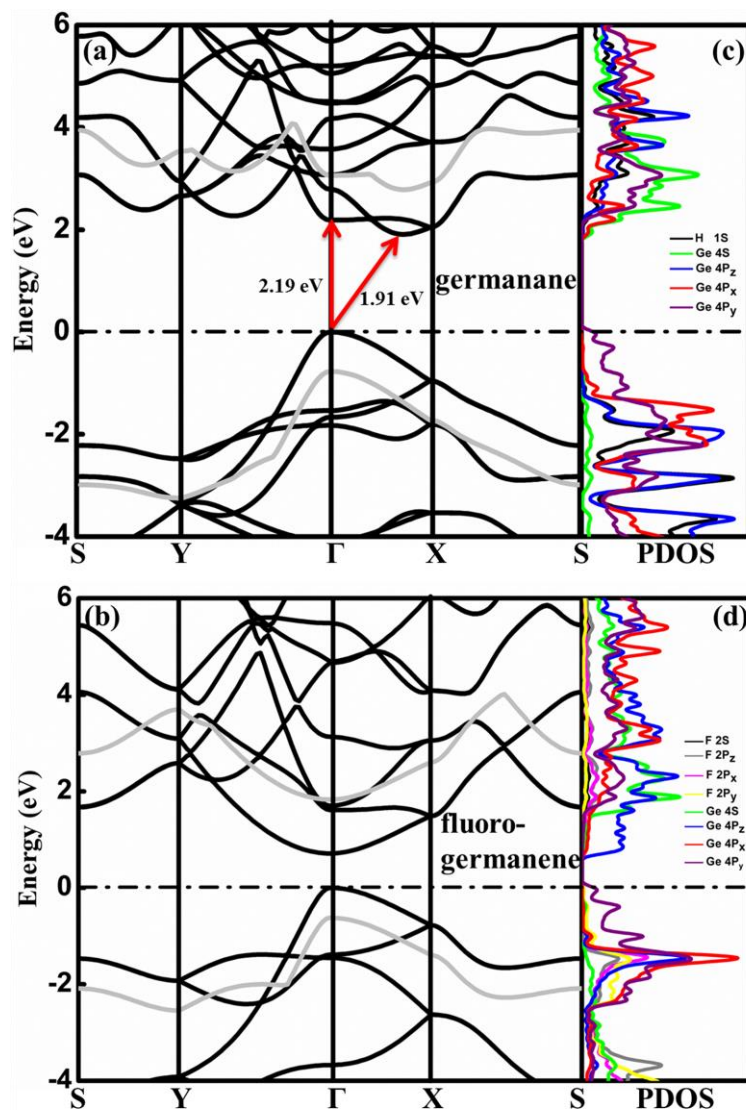


Figure 4. (a), (b): Band structures of germanane and fluorogermanene in Z-line configuration from LDA (black solid lines). The grey solid lines represent QP energies corrections to the LDA energies at relevant k -points of the uppermost valence band and the lowest conduction band. The energy of VBM is shifted to zero.

(c), (d): The projected density of states of germanane and fluorogermanene in Z-line configuration.

We now focus on the cases of the Z-line germanane and fluorogermanene with higher buckling. Their electronic band structures at LDA level, projected density of states and representative bands at *GW* level are presented in Figure 4. For germanane, hydrogenation induces an indirect band-gap of 1.91 eV between the Γ point and X point around (see Figure 4(a)). Moreover, the VBM is mainly derived from Ge-4 p_y orbital; while the CBM is mostly from Ge 4 s and 4 p_x orbitals (see Figure 4(c)). For fluorogermanene, the VBM is dominated from Ge-4 p_y and F-2 p_y orbitals; while the CBM is composed of Ge-4 p_z orbital (see Figure 4(d)). A direct band-gap of 0.71 eV is obtained at the Γ point, as shown in Figure 4(b). After considering quasi-particle corrections, the indirect (direct) band-gap increases to 3.65 eV (2.45 eV) for germanane (fluorogermanene). Such quasi-particle corrections to the LDA energy band are also the result of reduced dimension and rather weak electronic screening.

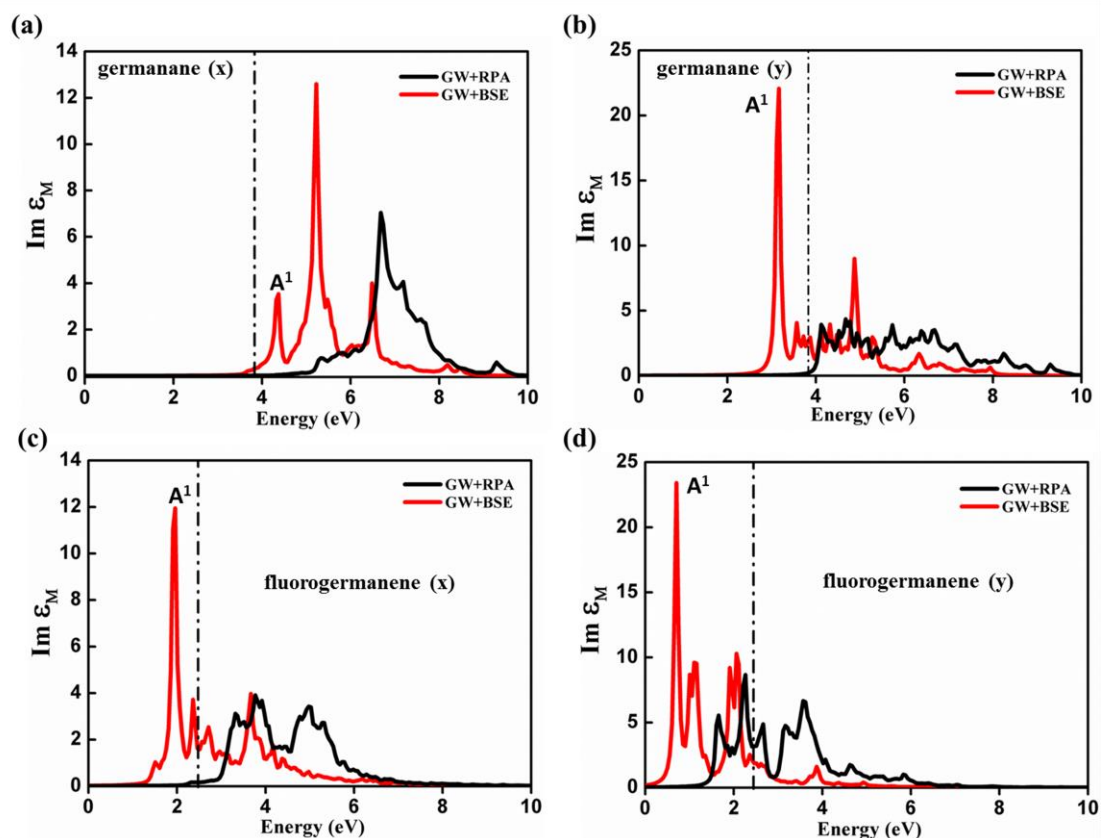


Figure 5. Optical absorption spectra for the incident light polarized along the x direction: (a), (c); y direction: (b), (d), in germanane and fluorogermanene. Without (black line) and with (red line) the e-h interaction, *i.e.* $GW+RPA$ and $GW+BSE$. The vertical black dash dot lines refer to the QP gap at the Γ point. A 0.05 eV Lorentzian broadening is employed in these plots.

Optical absorption spectra of the Z-line germanane and fluorogermanene are plotted in Figure 5. Quasi-particle corrections without and with e-h interaction are both considered, where the light is polarized along the x or y direction shown in Figure 1(c). When the self-energy corrections ($GW+RPA$) are included, the entire spectrum is blue-shift in comparison with that obtained in the independent-particle approximation; however, once the e-h interactions ($GW+BSE$) are included, the entire spectrum is

red-shift relative to that of $GW+RPA$. When the light is polarized along the x or y direction, the optical absorption spectra exhibit evident difference (see Figure 5(a)-5(d)). The germanane strongly absorbs y-polarized light in the energy range of 2.6 to 3.6 eV and is transparent to x-polarized light in this range, which is the result of selection rules associated with the symmetries of the anisotropic material. However, the fluorogermanene shows a strong absorption towards y-polarized light in the range of 0.3 ~ 1.5 eV and is transparent to x-polarized light.

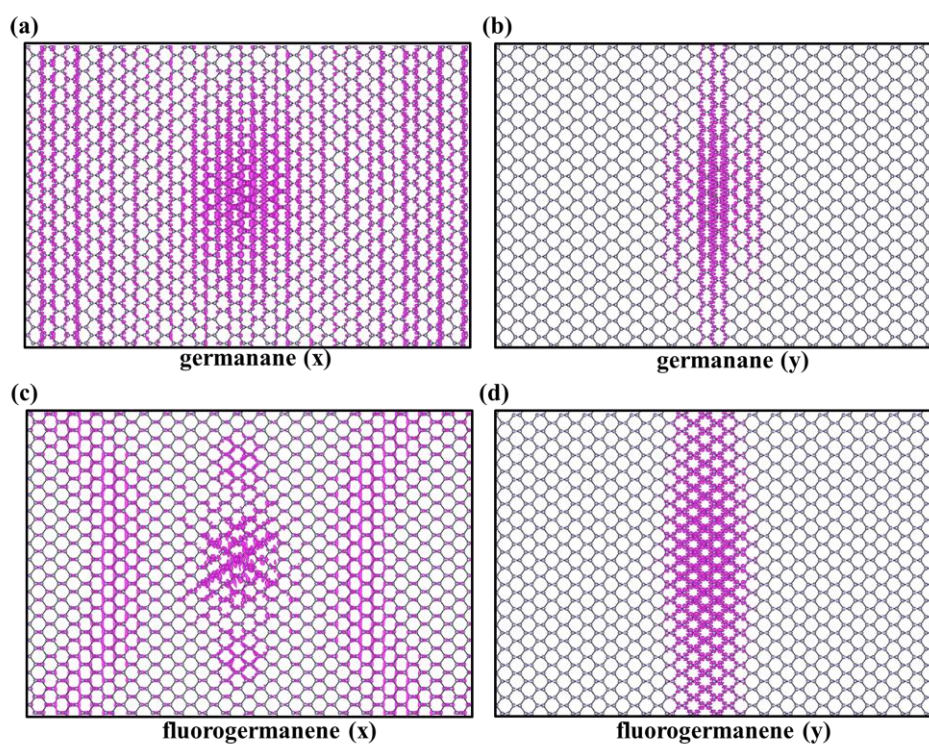


Figure 6. Top views of the real-space exciton distribution corresponding to the first absorption peaks along x-polarized light direction: (a), (c); y-polarized light: (b), (d), in germanane and fluorogermanene.

The position of the first absorption peak and its corresponding binding energy of germanane are listed in Table 2. When the x-polarized light is used in germanane, the

first absorption peak is observed at 4.33 eV. This is a resonant excitation, which is mostly contributed by the dipole-allowed vertical transitions between the top valence band to the first conduction band at X-point. The spatial distribution of the resonant exciton wave function is shown in Figure 6(a) and it spreads over a larger area. Moreover, the binding energy of the first resonant exciton (A^1) is 0.42 eV. When the y-polarized light is used, the first absorption peak locates at 3.15 eV, which is an optically active exciton (A^1) with the binding energy of 0.95 eV. Different from the resonant exciton aforementioned, the bound exciton wave function mainly distributes along zigzag direction of the lattice (see Figure 6(b) which the spatial distribution of the bound exciton wave function is presented), indicating anisotropic optical response. The large binding energy of exciton in germanane is the result of weak and nonlocal dielectric screening. For fluorogermanene, the first bound exciton (A^1) locates at 1.94 eV, which is an optically active exciton with the bound energy as large as 2.37 eV. When y-polarized light is applied in fluorogermanene, the first absorption peak is observed at 0.72 eV, the corresponding exciton has a binding energy of 2.80 eV. The spatial distribution of the two bound excitons wave function show similar profiles as germanane (see Figure 6(c)-(d)). The large bound energy together with their highly anisotropic optical responses observed in germanane and fluorogermanene are of particular interest and may be good optical linear polarizers.

4 Conclusions

In summary, the structural stabilities, electronic and optical properties of germanane and fluorogermanene have been investigated within the framework of density

functional theory, G_0W_0 method and Bethe-Salpeter equation. The chair and zigzag-line configurations are energetically preferred for both the germanane and fluorogermanene. The chair germanane and fluorogermanene and zigzag-line fluorogermanene exhibit direct band-gaps, while the zigzag-line germanane is an indirect-gap semiconductor. Furthermore, the significant quasi-particle corrections and strong excitonic effects with large exciton binding energies are observed. More interestingly, highly anisotropic optical responses are observed in zigzag-line germanane and fluorogermanene. Absorption spectrum of x-polarized light dominates over high energy region in germanane, while that of y-polarized light is predominant in low energy region in germanane and fluorogermanene. These interesting electronic and optical properties of germanane/fluorogermanene and the fundamental understandings are potentially useful for future optoelectronic device design.

Acknowledgements

This work is supported by the NBRP (2011CB302004), NSF (21173040, 21373045) and of Jiangsu (BK20130016) and SRFDP (20130092110029) in China. The authors thank the computational resources at the SEU and National Supercomputing Center in Tianjin.

References

1. K. S. Novoselov, A. K. Geim, S. V. Morozov, D. Jiang, M. I. Katsnelson, I. V. Grigorieva, S. V. Dubonos, and A. A. Firsov, *Nature*, 2005, **438**, 197.

2. A. K. Geim and K. S. Novoselov, *Nature Mater.*, 2007, **6**, 183.
3. C. G. Lee, X. D. Wei, J. W. Kysar, and J. Hone, *Science*, 2008, **321**, 385.
4. C. N. R. Rao, A. K. Sood, K. S. Subrahmanyam and A. Govindaraj, *Angew. Chem. Int. Ed.*, 2009, **48**, 7752.
5. F. Schedin, A. K. Geim, S. V. Morozov, E. W. Hill, P. Blake, M. I. Katsnelson, and K. S. Novoselov, *Nature materials*, 2007, **6**, 652.
6. F. Bonaccorso, Z. Sun, T. Hasan, and A. C. Ferrari, *Nature photonics*, 2010, **4**, 611.
7. D. W. Boukhvalov, M. I. Katsnelson, and A. I. Lichtenstein, *Phys. Rev. B*, 2008, **77**, 035427.
8. M. S. Fuhrer, C. N. Lau, and A. H. MacDonald, *MRS Bulletin*, 2010, **35**, 289.
9. R. Balog, B. Jørgensen, L. Nilsson *et al.*, *Nature Mater.*, 2010, **9**, 315.
10. J. T. Robinson, J. S. Burgess *et al.*, *Nano Lett.*, 2010, **10**, 3001.
11. J. O. Sofo, A. S. Chaudhari, G. D. Barber, *Phys. Rev. B*, 2007, **75**, 153401.
12. D. C. Elias, R. R. Nair, T. M. G. Mohiuddin *et al.*, *Science*, 2009, **323**, 610.
13. R. R. Nair, W. Ren, R. Jalil, I. Riaz *et al.*, *Small*, 2010, **6**, 2877.
14. H. Liu, S. Ryu, Z. Chen, M. L. Steigerwald, C. Nuckolls and L. E. Brus, *J. Am. Chem. Soc.*, 2009, **131**, 17099.
15. F. M. Koehler, A. Jacobsen, K. Ensslin, C. Stampfer and W. J. Stark, *Small*, 2010, **6**, 1125.
16. S. Ryu, M. Y. Han, J. Maultzsch, T. F. Heinz, P. Kim, M. L. Steigerwald, L. E. Brus, *Nano Lett.*, 2008, **8**, 4597.
17. H. Kim, H. H. Kim, J. I. Jang, S. K. Lee, G. W. Lee, J. T. Han, and K. Cho, *Adv.*

- Mater.*, 2014, doi: 10.1002/adma.201403196.
18. S. Cahangirov, M. Topsakal, E. Aktürk, H. Sahin, S. Ciraci, *Phys. Rev. Lett.*, 2009, **102**, 236804.
19. Y. Ding and J. Ni, *Appl. Phys. Lett.*, 2009, **95**, 083115.
20. S. Cahangirov, M. Topsakal, S. Ciraci, *Phys. Rev. B*, 2010, **81**, 195120.
21. S. Wang, *Phys. Chem. Chem. Phys.*, 2011, **13**, 11929.
22. L. C. Lew Yan Voon, E. Sandberg, R. S. Aga, and A. A. Farajian, *Appl. Phys. Lett.*, 2010, **97**, 163114.
23. J. C. Garcia, D. B. de Lima, L. V. C. Assali, and J. F. Justo, *J. Phys. Chem. C*, 2011, **115**, 13242.
24. A. O'Hare, F. V. Kusmartsev, and K. I. Kugel, *Nano Lett.*, 2012, **12**, 1045.
25. F. Bechstedt, L. Matthes, P. Gori and O. Pulci, *Appl. Phys. Lett.*, 2012, **100**, 261906.
26. B. Lalmi, H. Oughaddou, H. Enriquez, A. Kara, S. Vizzini, B. Ealet, and B. Aufray, *Appl. Phys. Lett.*, 2010, **97**, 223109.
27. M. E. Dávila, L Xian, S. Cahangirov, A. Rubio, and G. Le Lay, *New J. Phys.*, 2014, **16**, 095002.
28. M. Houssa, E. Scalise, K. Sankaran, G. Pourtois, V. V. Afanašev, and A. Stesmans, *Appl. Phys. Lett.*, 2011, **98**, 223107.
29. Y. Ding and Y. Wang, *Appl. Phys. Lett.*, 2012, **100**, 083102.
30. W. Wei and T. Jacob, *Phys. Rev. B*, 2013, **88**, 045203.
31. O. Pulci, P. Gori, M. Marsili, V. Garbuio, R. Del Sole, F. Bechstedt, *Europhys.*

- Lett.*, 2012, **98**, 37004.
32. J. P. Perdew and Y. Wang, *Phys. Rev. B*, 1992, **45**, 13244.
33. P. Giannozzi, S. Baroni *et al.*, *J. Phys.: Condens. Matter*, 2009, **21**, 395502.
34. N. Troullier and J. L. Martins, *Phys. Rev. B*, 1991, **43**, 1993.
35. L. Hedin, *Phys. Rev.*, 1965, **139**, A796.
36. L. Hedin and S. Lundqvist, *Solid State Physics*, 1970, **23**, 1.
37. M. S. Hybertsen and S. G. Louie, *Phys. Rev. B*, 1986, **34**, 5390.
38. A. Marini, C. Hogan, M. Grüning, and D. Varsano, *Comput. Phys. Commun.*, 2009, **180**, 1392.
39. R. W. Godby and R. J. Needs, *Phys. Rev. Lett.*, 1989, **62**, 1169.
40. A. Oshlies, R. W. Godby, and R. J. Needs, *Phys. Rev. B*, 1995, **51**, 1527.
41. M. Rohlfing and S. G. Louie, *Phys. Rev. B*, 2000, **62**, 4927.
42. Salpeter and Bethe, *Phys. Rev.*, 1951, **84**, 1232.
43. G. Onida, L. Reining, A. Rubio, *Rev. Mod. Phys.*, 2002, **74**, 601.
44. X. Wen, L. Hand, V. Labet, T. Yang, R. Hoffmann, N. W. Ashcroft, A. R. Oganov, and A. O. Lyakhov, *Proc. Natl. Acad. Sci. U.S.A.*, 2011, **108**, 6833.
45. H. Sahin, S. Cahangirov, M. Topsakal, E. Bekaroglu, E. Akturk, R. T. Senger and S. Ciraci, *Phys. Rev. B*, 2009, **80**, 155453.
46. G. Vogg, M. S. Brandt, and M. Stutzmann, *Adv. Mater.*, 2000, **12**, 1278.
47. E. Bianco, S. Butler, S. Jiang, O. D. Restrepo, W. Windl, and J. E. Goldberger, *ACS Nano*, 2013, **5**, 4414.
48. O. Leenaerts, H. Peelaers, A. D. Hernández-Nieves, B. Partoens, and F. M. Peeters,

Phys. Rev. B, 2010, **82**,195436.

49. P. Cudazzo, C. Attaccalite, I. V. Tokatly, and A. Rubio, *Phys. Rev. Lett.*, 2010, **104**
226804.

50. C. D. Spataru, S. Ismail-Beigi, L. X. Benedict, and S. G. Louie, *Phys. Rev. Lett.*,
2004, **92**, 077402.

51. F. Wang, G. Dukovic, L. E. Brus, and T. F. Heinz, *Science*, 2005, **308**, 838.

52. L. Yang, M. L. Cohen, and S. G. Louie, *Nano Lett.*, 2007, **7**, 3112.

53. D. Y. Qiu, F. H. da Jornada, and S. G. Louie, *Phys. Rev. Lett.*, 2013, **111**, 216805.

54. W. Wei, Y. Dai, B. Huang and T. Jacob, *Phys. Chem. Chem. Phys.*, 2013, **15**, 8789.